Science of the Total Environment 1019 (2026) 181551

Contents lists available at ScienceDirect

Science of the Total Environment

journal homepage: www.elsevier.com/locate/scitotenv

Impact of volcanic emissions on the air quality during the 2021 volcanic eruption of Tajogaite, La Palma: Implications for population exposure to volcanic pollutants

Julia Eychenne [a,b,*], Raphael Paris [a], Agnès Borbon [c], David Jessop [a], Mathieu Gouhier [a], Guillem Gisbert Pinto [d,e], Antoni Calafat [f], Aurélie Colomb [c], José-Luis Fernandez-Turiel [g], Vincent Gaussen [a], Clara Gorce [a], Séverine Moune [a], Wilman Navarrete [a,h], Jean-Marie Nedelec [i], Alejandro Rodriguez-Gonzalez [j], Ines Tomašek [a,b], Jon Vilches [k], Francisco Jose Perez-Torrado [j]

[a] Université Clermont Auvergne, CNRS, IRD, OPGC, Laboratoire Magmas et Volcans, F-63000, Clermont-Ferrand, France
[b] Université Clermont Auvergne, CNRS, INSERM, Institut Génétique, Reproduction et Développement, F-63000, Clermont-Ferrand, France
[c] Université Clermont Auvergne, CNRS, LaMP, OPGC, Clermont-Ferrand, France
[d] Departament de Mineralogia, Petrologia i Geologia Aplicada, Universitat de Barcelona, Barcelona, 08028, Spain
[e] Geomodels Research Institute. Universitat de Barcelona, Martí Franquès s/n, 08028 Barcelona, Spain
[f] Departament de Dinàmica de la Terra i de l'Oceà, Universitat de Barcelona, Barcelona, 08028, Spain
[g] Geosciences Barcelona, GEO3BCN, CSIC, Barcelona, Spain
[h] Université de Lille, CNRS, IRD, Université Littoral Côte d'Opale, Laboratoire d'Océanologie et de Géosciences, Lille, France
[i] Université Clermont Auvergne, Clermont Auvergne INP, CNRS, ICCF, F-63000, Clermont-Ferrand, France
[j] Instituto de Estudios Ambientales y Recursos Naturales (i-UNAT), Universidad de Las Palmas de Gran Canaria (ULPGC), Las Palmas de Gran Canaria, Spain
[k] Department of Ecological Transition, Fight against Climate Change and Territorial Planning, Canary Islands Government, Spain

HIGHLIGHTS

- Ambient air quality was degraded during the 2021 Tajogaite eruption.
- Ambient air pollution peaks are related to episodes of high tephra deposition rates.
- Secondary aerosol formation contributed little to the PM load.
- Low-explosivity basaltic eruptions can generate sub-10 μm volcanic ash.
- Elevated PM concentrations persist longer than intense tephra deposition episodes.

GRAPHICAL ABSTRACT

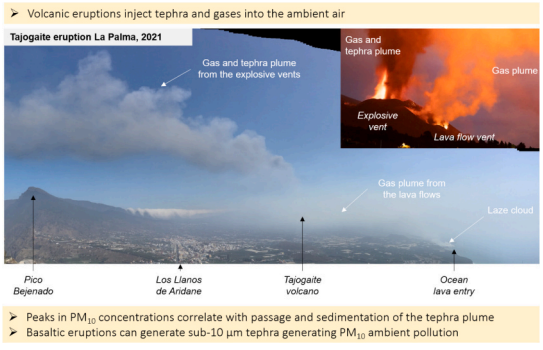

ARTICLE INFO

Keywords:
Volcanic eruption
Air quality
PM pollution peaks

ABSTRACT

Volcanic eruptions inject particles (tephra) and gases into the atmosphere, impacting air quality. To provide new insights into this process, we focus on the 3-month-long 2021 Tajogaite eruption, on La Palma in the Canary Islands, Spain. This eruption emplaced lava flows and produced tephra and gases in multiple sustained plumes.

* Correspondig author at: Université Clermont Auvergne, CNRS, IRD, OPGC, Laboratoire Magmas et Volcans, F-63000, Clermont-Ferrand, France.
E-mail address: julia.eychenne@uca.fr (J. Eychenne).

https://doi.org/10.1016/j.scitotenv.2026.181551
Received 3 November 2025; Received in revised form 6 February 2026; Accepted 11 February 2026
Available online 17 February 2026

Tephra deposition
Population exposure

We examined the relationship between air quality, tephra dispersion and deposition, and eruption dynamics. We reconstructed the spatiotemporal variations in tephra deposition using a collection network deployed around the island and maintained throughout the eruption, while plume dispersion was tracked using satellite observations. These datasets were compared to the air quality monitoring data from the local regulatory network using time-series analyses.

Our findings reveal distinct peaks in tephra deposition rates (a few $g/m^2/h$ 20 km away from the vent, up to more than 2000 $g/m^2/h$ at locations less than 3 km from the vent), related to both increased explosive activity at the volcanic vents and specific atmospheric conditions. We show that the fluctuations of tephra emission were the main driver of the particulate matter (PM) concentration variations, outweighing contributions from secondary aerosol formation through volcanic SO_2 conversion. We evidence spatial disparity in the impact on air quality, with the western half of La Palma island experiencing higher amplitude and more frequent pollution peaks than the eastern half. We demonstrate that even low-explosivity basaltic eruptions can significantly affect air quality by generating and dispersing fine PM and gases over wide areas. Moreover, elevated PM concentrations persist beyond the duration of intense tephra deposition episodes, thereby extending the period of population exposure. These results have important implications for understanding and mitigating human exposure to volcanic pollutants.

1. Introduction

Volcanic eruptions inject large quantities of gas and tephra (solid particles formed by magma fragmentation and ejection at the vent) into the atmosphere. These volcanic emissions can affect the air quality at ground level (i.e. up to a few meters above the ground), and pose a threat to nearby populations upon inhalation. Fine particle air pollution is indeed a major public health concern worldwide, contributing to more than 8 million premature deaths in 2021, primarily from respiratory and cardiovascular disease, according to the 2024 State of Global Air report (Health Effect Institute, 2024). As more than 1 billion people live within 100 km of a volcano active in the Holocene (Freire et al., 2019), it is critical to understand the extent to which volcanic emissions impact air quality.

Volcanic emissions are dispersed to varying altitudes and distances, depending on eruption dynamics such as the depth and efficiency of magma fragmentation, the mass eruption rate of tephra (eruption intensity), the prevailing atmospheric conditions. During transport in the atmosphere, they undergo diverse post-eruptive physicochemical processes. These include the oxidation and transformation of volcanic gas species into aerosol particles (Mather et al., 2003; Textor et al., 2003), interactions between gases, aerosols and tephra surfaces (Delmelle et al., 2007; Delmelle et al., 2018), and exchanges with the background atmosphere that contains other natural or anthropogenic aerosols (Tomašek et al., 2021). As emissions settle, they follow individual or collective sedimentation regimes that depend on particle size, shape and density, on particle concentration in the plume, on atmospheric conditions, and on the surface topography (e.g., Manzella et al., 2015; Rose and Durant, 2011; Saxby et al., 2018; Sparks et al., 1992). These complex spatiotemporal mechanisms of dispersion, transformation, and sedimentation make volcanic emissions a highly variable source of air pollution, posing significant difficulties for prediction and assessment.

Ambient air quality is monitored throughout the world, mostly in populated areas, via regulatory monitoring networks. These air quality stations provide hourly to daily concentration measurements of various particulate and gas species, including particulate matter (PM) finer than 10 and 2.5 μm in size (PM_{10} and $PM_{2.5}$, respectively), and SO_2, NOx and CO gases. These networks are primarily designed to monitor air quality in relation to anthropogenic sources; hence stations are rarely located at appropriate sites to closely monitor air pollution due to volcanic eruptions. Despite these limitations, analyses of regulatory air quality data as well as information from low-cost air quality sensors in volcanic environments have provided growing evidence that air quality is degraded during volcanic eruptions (e.g., Searl et al., 2002; Carlsen et al., 2015; Milford et al., 2023), most clearly associated with SO_2 plumes and SO_2-derived aerosols (Whitty et al., 2020). However, the degree and mechanisms by which volcanic emissions contribute to PM_{10} and $PM_{2.5}$ air concentration levels during eruptions remain open questions. Potential sources of volcanic PM include aerosols formed from the transformation of volcanic gases and volcanic ash (i.e. tephra smaller than 2 mm with size distributions extending into the nanometer range). During volcanic eruptions, volcanologists quantify the production and dispersion of volcanic emissions by measuring tephra deposition, the concentration and composition of volcanic gases in the air close to the vents, and by tracking the dispersion of the gas and tephra in the atmosphere through satellite remote sensing. Yet these datasets have rarely been correlated with air quality monitoring records (Milford et al., 2023; Whitty et al., 2020). Establishing such links would make it possible to trace PM pollution peaks to specific volcanic sources and eruption processes, and to test which volcanological parameters are appropriate proxies of air pollution.

To provide new insights into the impact of tephra sedimentation on ambient air quality, we studied the 3-month-long 2021 Tajogaite eruption, on the island of La Palma in the Canary Islands (Spain). This eruption was a case example of a hybrid basaltic eruption, i.e. an eruption with sustained gas and tephra plumes produced simultaneously with the emplacement of lava flows (Bonadonna et al., 2022). This eruption style has been observed at other basaltic centers such as Paricutin, Mexico (Pioli et al., 2008) and Etna, Italy (Taddeucci et al., 2002). Despite its low intensity, the Tajogaite eruption had a major impact on the population of the island, due to the destruction caused by the deposition of tephra, the emplacement of a large lava flow field in an inhabited area, and disruption due to its extended duration (Biass et al., 2024; Carracedo et al., 2022). In addition to these direct impacts on buildings and infrastructures, the Tajogaite eruption repeatedly degraded air quality, forcing population confinements (i.e. cessation of public activities and population advised to stay indoors) as a precaution against negative health effects (Carracedo et al., 2022). This demonstrates that low-intensity basaltic eruptions can significantly affect air quality through the production and dispersion of fine PM and gas.

Here, we explore how and through which processes the Tajogaite eruption impacted air quality, by analysing the relationship between air quality, tephra dispersion and sedimentation, and eruption dynamics. We reconstruct tephra deposition time series across La Palma using a tephra collection network deployed all around the island and maintained throughout the eruption, with plume dispersion dynamics retrieved from satellite observations. These datasets were compared to the air quality monitoring data from the Government of the Canary Islands regulatory network using qualitative and quantitative time-series analyses. Our findings reveal maxima in tephra deposition rates related to both increased explosive activity and specific atmospheric conditions and also show that the tephra deposition rate was the main driver of PM concentration variations in the ambient air during the eruption. Our work provides new insights for the contribution of tephra plumes to air quality during hybrid basaltic eruptions and their implications for human exposure to volcanic pollutants.

2. Background on the 2021 Tajogaite eruption

Historical volcanic eruptions in the Canary Islands have been Strombolian-Hawaiian hybrid eruptions of moderate explosivity (including some phreatomagmatic phases due to the interaction of the ascending magma with groundwater), forming tephra cones and lava flows typical of this eruption style. Although tephra falls associated with these eruptions are clearly mentioned in historical accounts, this hazard is poorly documented (Longpré and Felpeto, 2021). Of the 16 historical eruptions recorded in the archipelago since 1480, half occurred along the Cumbre Vieja. The eruptions of 1949 and 1971 have been relatively well described (Afonso et al., 1974; Bonelli Rubio, 1950), but seismic, geodetic, and geochemical monitoring networks were only set up towards the end of the 20th century. The underwater eruption south of the island of El Hierro in 2011–2012 was the first volcanic eruption documented with modern instrumental techniques in the Canary Islands (e.g., Martí et al., 2013; Somoza et al., 2017). Ten years after the El Hierro event, the Tajogaite eruption was monitored in an unprecedented way by the scientific community.

The eruption of Tajogaite volcano lasted 86 days, from 19 September to 13 December 2021. It was characterized by a sustained low-intensity explosive activity (average tephra mass eruption rate of 3–4 $\times$ 10^3 kg/s; Bonadonna et al., 2022) at one or more summit craters, and consisting in fountaining and/or strombolian style explosions (Bonadonna et al., 2023) and the synchronous emplacement of lava flows from a vent at the base of the explosive cones (Plank et al., 2023) (see Graphical Abstract).

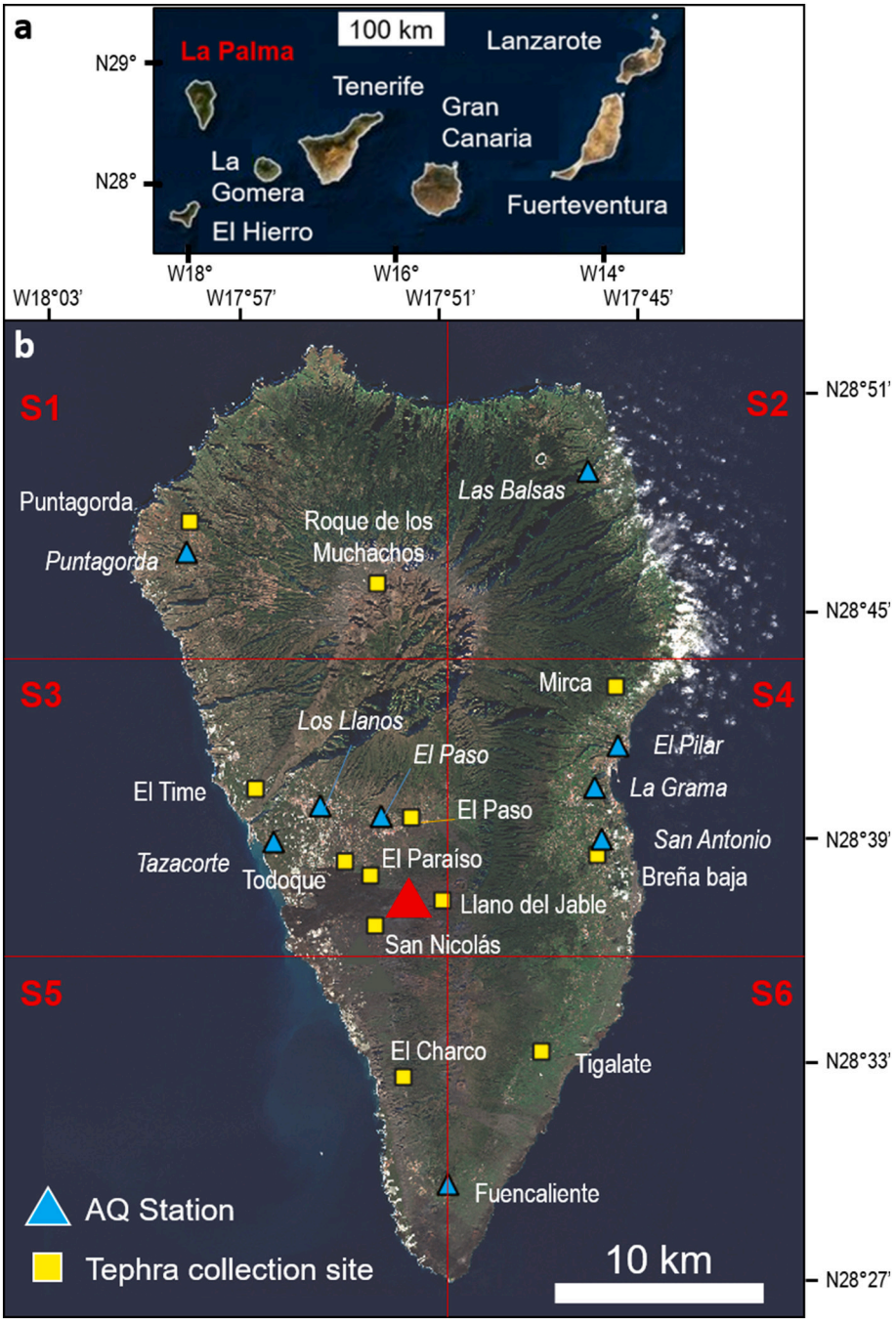

Fig. 1. (a) Location of La Palma in the Canary Islands archipelago. (b) Location of Tajogaite volcano (red triangle), the air quality stations (blue triangles), tephra collection sites (yellow squares), and sectors defined for satellite observations (S1 to S6 in red). Images Landsat Copernicus from Google Earth.

A tephra blanket several centimeters-thick formed in the south-west part of the island (Bonadonna et al., 2022), but tephra dispersed and deposited all around the island at different times of the eruption (Shatto et al., 2024), sometimes spreading as far as the islands of El Hierro and Gran Canaria, 90 km to the south and 220 km to the east, respectively (see Fig. 1a for locations). Intense volcanic gas emissions occurred during the eruption, with dilute plumes forming at the lava flow vent and the degassing lava flow field, and from the plumes associated with fountaining and strombolian activity at the explosive vents (see Graphical Abstract; Asensio-Ramos et al., 2025). Lava flows reached the shore a few days within the eruption, forming sporadic haze plumes (often referred to as laze) due to the lava entering the ocean and vaporizing seawater. Overall, the eruption produced $54.7 \pm 23.9 \times 10^{10}$ kg of magma, including $6.9 \pm 0.514 \times 10^{10}$ kg in tephra fall deposits and $47.8 \pm 23.5 \times 10^{10}$ kg in lava flows (Bonadonna et al., 2022), making it the third largest historical eruption in the Canary Islands and also one of the longest. The eruption also injected a total of 110.7 ± 57.6 kt of SO_2 into the atmosphere (Burton et al., 2023).

Total damage associated with the eruption approaches one billion euros according to the Government of the Canary Islands (https://www3.gobiernodecanarias.org/noticias/la-erupcion-de-la-palma-se-declara-finalizada-tras-85-dias-y-8-horas-de-duracion-y-1-219-hectareas-de-coladas/). Lava flows had the greatest impact, covering an area of 12.2 km^2, destroying over 2000 buildings, cutting 74 km of roads and rendering 370 ha of farmland unusable (including 229 ha of banana plantations, the island's main economic sector along with tourism). Seven thousand people had to be evacuated, while thousands of others went through several phases of confinement due to ash and gas emissions in the ambient air. Tephra covered 624 ha of farmland. The cumulative thickness of tephra reaches several meters around the volcano. The 10 cm isopach describes a 4 × 7 km ellipse oriented southwest-northeast, while the 1 cm isopach covers a large part of the southern half of the island (Bonadonna et al., 2022; Shatto et al., 2024).

3. Data and methods

3.1. Tephra collection network

Within a few days of the eruption, we had deployed a network of tephra collectors (plastic trays of known dimensions, see Fig. S1 in Supplementary Information). The collectors were located at 12 different locations around the island (Fig. 1b), and sampled by the authors or volunteers every 24 h over the course of several days. The time and date of collection were carefully recorded and collection durations were calculated from these. We also recorded observations of the weather, wind direction, and direction of the plume. The full sample database is presented as Table S1 in the Supplementary Information.

3.2. Physical characterization of the tephra samples

All tephra samples were dried overnight at 60 °C in a laboratory oven and subsequently weighed. The mass per unit area (MpUA) of tephra deposited was calculated using the dimensions of the collection trays (typically 43 × 26 × 8 cm). Tephra deposition rates, corresponding to the mass of tephra falling over time onto a given surface area (MpUA per unit time), were also determined using the collection durations (Table S1).

Particle size distributions of a selection of samples (spaced out evenly over time) from 10 collection sites (Table S1 in Supplementary Information) were measured by sieving at half phi intervals (phi = $-\log_2$(particle diameter in mm)), or by sieving and laser diffraction analysis for particles finer than 63 μm, or by laser diffraction analyses only when no particles coarser than 2 mm were present in the samples. When only laser diffraction was used, we express the resulting distributions in vol%, while when sieving and laser diffraction were combined we use wt%. The merged sieving and laser diffraction wt% distribution is obtained assuming that all the particles finer than 63 μm have the same density and normalizing the vol% distribution from laser diffraction to the mass of the sub-63 μm fraction obtained by sieving. Laser diffraction analyses were performed using a Malvern Mastersizer 2000 at Sigma (UCA, Clermont-Ferrand), and a Beckman Coulter LS230 at the Facultat de Ciències de la Terra (UB, Spain). The absorption coefficient and refractive index were set at 0.1 and 1.6, respectively. We report the median (50th quantile) and the sorting (half the difference between the 84th and 16th quantiles) for the particle size distributions (Table S1).

3.3. Satellite observation of the dispersion of the tephra plume

Tephra plume dispersion over the La Palma island from 19 September to 13 December 2021 was characterized using datasets from both thermal infrared (high temporal resolution and low spatial resolution) and visible (low temporal resolution and high spatial resolution) satellite remote sensing.

Thermal infrared satellite images were acquired with the SEVIRI instrument on board the MSG satellite, and accessed through the HOTVOLC observing system (https://hotvolc.opgc.fr/). Over La Palma, thermal infrared images have a spatial resolution of ~3 km × 3 km, and temporal resolution of 15 min. For each image, we recorded the presence or absence of the plume above the six predefined sectors covering the entire island (Fig. 1b). We considered only the tephra plume, which appears as a dark blue shape on false RGB images and usually highlighted by using both 2 and 3-band algorithms available on the HOTVOLC web-SIG interface. This approach does not allow detection of optically thin (i.e. dilute) or water-rich plumes (Guéhenneux and Gouhier, 2024). Final identification of the plume was performed manually, guided by contextual information such as plume shape, the location of the volcanic vent, and dispersion dynamics. Assuming each image represented the position of the plume for the past 15 min, we then calculated for each day of the eruption, the percentage of time that a tephra plume was dispersed above each sector (Table S2 in Supplementary Information).

Visible images acquired by the MODIS instruments on board the Terra and Aqua satellites were also studied by visual inspection using the tool Worldview of NASA (https://worldview.earthdata.nasa.gov/). One image was acquired per satellite per day. Over La Palma, these images have a spatial resolution of 500 m × 500 m, which is sufficient to allow dilute and small/narrow plumes to be detected. From these images, we noted the presence of a tephra plume, its position relative to the six sectors mentioned above, and the acquisition time. These data are also presented in Table S2.

3.4. Air quality and meteorological data

A regulatory air quality (AQ) monitoring network is maintained by the Government of the Canary Islands (data available at https://www3.gobiernodecanarias.org/medioambiente/calidaddelaire/inicio.do). Four stations located in the west of the island had been established prior to the eruption, and five additional stations in the east and south of the island were added during the course of the eruption thanks to efficient inter-agency coordination as part of the emergency response (Fig. 1b). All stations systematically recorded 1-hour mean SO_2 ambient air concentrations (in $\mu g/m^3$) as well as air temperature, pressure, humidity, and wind speed and direction. Some stations also recorded 1-hour mean PM_{10} and $PM_{2.5}$ ambient air concentrations, as well as CO, O_3, NO_2, and NO concentrations. The parameters measured, as well as the periods of the eruption covered by the measurements, are summarized in Table S3 in Supplementary Information. The 1-hour mean AQ data were averaged to 24-hour means in this work (Table S4 in Supplementary Information). Meteorological information (1-hour mean data) from the AEMET (Agencia Estatal de Meteorologia, Spain) weather station at the Roque de Los Muchachos Astronomical Observatory (Fig. 1b) was also compiled for the eruption period (Table S5 in Supplementary

Information).

To examine potential correlations between AQ datasets, the time series of the 24-hour mean concentrations of SO_2, PM_{10}, and $PM_{2.5}$ were analysed using auto- and cross-correlation, computed with the *correlate* and *correlation_lags* functions from the Python *scipy.signal* library. Cross-correlation between two time series, *a* and *b*, quantifies their similarity as a function of temporal offset. Auto-correlation, by contrast, measures the similarity of a time series with itself at different lags and is commonly used to detect periodicities. We normalized the time series so that the correlation values fall in the range [-1, 1], where +1 indicates perfect correlation, -1 perfect anti-correlation, and 0 no correlation.

4. Results

4.1. Tephra deposition rates

Tephra deposition rate variations at the 12 collection sites (Fig. 2) show a general decrease from the most proximal collection sites (El Paraíso, San Nicolás and Llano del Jable, located less than 3 km from vents to the North-West, South-West and East respectively) to the most distal sites (up to 21 km away from the volcano). Deposition rates as high as 2500 g/m^2/h were recorded at the proximal sites, while rates smaller than 10 g/m^2/h were recorded at the distal sites (Fig. 2). This observation is in agreement with the depletion in tephra of the volcanic plume during transport in the atmosphere. Deposition rates decreased over time during the course of the eruption at the three proximal collection sites, as evidenced by the decrease both in amplitude and frequency of the maxima in deposition rates at these sites (Fig. 2).

Although the time series of tephra deposition rates exhibit distinct trends at each of the 12 collection sites (Fig. 2), maxima are often correlated across multiple sites (highlighted in Fig. 2 and listed in Table S6, Supplementary Information). We distinguish two scenarios (Fig. 2): (1) maxima occur at one of the three proximal sites and, in some cases, are also observed at distal sites (21–26 Sept., 04–08 Oct., 26–29 Oct., 30 Oct.-02 Nov., and 24–26 Nov.); (2) maxima occur at distal sites without corresponding maxima at proximal sites (01 Oct., 16 Oct., 05 Nov., 14–17 Nov., and 09–14 Dec.).

4.2. Air quality

Air quality monitoring data for SO_2, PM_{10} and $PM_{2.5}$ concentrations showed significant variations at stations where data were available (Fig. 3). Compared to the same period in 2020, 2022 and 2023 (Fig. S2 in Supplementary Information), a notable increase in SO_2 concentrations occurred in 2021, and maxima in PM_{10} and $PM_{2.5}$ concentrations were more frequent. Clear correlations between PM_{10} and $PM_{2.5}$ time series are observed at all the stations where both contaminants were measured for the entire duration of the eruption, while no significant correlations between the PM and SO_2 time series are apparent at any lag (Fig. 4).

24-h mean SO_2 concentrations exceeded 100 μg/m^3 several times during the eruption at Los Llanos, Puntagorda, El Paso, and Tazacorte, with the Los Llanos and Puntagorda time series showing the highest background (Fig. 3). The World Health Organization (WHO) SO_2 concentration AQ guideline (24-hour mean of 40 μg/m^3) was exceeded at least once at all the stations except Las Balsas during the eruption. On several occasions, peaks in SO_2 ambient air concentration were simultaneously recorded at two or more stations (Fig. 3), irrespective of their location on the island (Fig. 1b).

PM_{10} and $PM_{2.5}$ 24-h mean concentrations above 100 and 20 μg/m^3, respectively, were reached several times during the eruption at Los Llanos with maxima of 400 and 60 μg/m^3, respectively (Fig. 3). This is the only AQ station in the western part of the island with a complete record of PM concentrations (Fig. 1b). It shows the highest PM concentration background of all the time series, with a clear decrease after mid-November (Fig. 3). The WHO AQ guidelines for PM_{10} and $PM_{2.5}$ (24-hour means of 45 and 15 μg/m^3, respectively) were exceeded at least twice at all stations that were active during the entire eruption (Las Balsas, El Pilar, La Grama, San Antonio, and Los Llanos). Similarly to SO_2 concentrations, simultaneous peaks in PM_{10} and $PM_{2.5}$ concentrations were observed at two or more stations (Fig. 3), including between Los Llanos and stations on the eastern side of the island (Fig. 1b). Although the rate of increase and maximum concentration differs at the various AQ stations, the periods in which elevated concentrations were observed are globally similar (Fig. 3). The most significant increases in PM concentration (highlighted in blue in Fig. 3) were recorded at: (1) Las Balsas (north-eastern station), El Pilar, La Grama, San Antonio (eastern stations) and Los Llanos (western station) on 27 Sept.-4 Oct., 14–21 Oct., and 3–5 Dec.; (2) El Pilar, La Grama and San Antonio (eastern stations) on 20–25 Nov.; (3) Los Llanos (western station) on 6–9 Oct., 30 Oct.-8 Nov., and on 10–17 Nov. These periods of elevated PM concentration are highlighted in Figs. 3 to 5 and listed in Table S7 in Supplementary Information.

NO_2 and CO (measured at El Pilar, La Grama, San Antonio, and Los Llanos; Fig. 1b) are gas species known for their anthropogenic origin (typically emitted by traffic and combustion) and not directly emitted by the volcanic activity. We included these species in our analysis as potential tracers of anthropogenic sources. Their ambient air 24-h mean concentrations remained relatively low during the Tajogaite eruption, except for notable peaks in NO_2 concentrations, 20 and 40 μg/m^3, in the periods 18–19 Oct. and 21–23 Nov., respectively (Fig. 3). On 18 Oct., NO_2 24 h-mean concentrations exceeding 50 μg/m^3 were observed at La Grama, accompanied by peaks in the SO_2 (lasting until 19 Oct.), $PM_{2.5}$ and PM_{10} 24 h-mean concentrations (Fig. 3). On 19 Oct., NO_2 24-h mean concentrations >25 μg/m^3 were observed at El Pilar and San Antonio, accompanied by peaks in SO_2, $PM_{2.5}$ and PM_{10} 24 h-mean concentrations at El Pilar, and a peak in SO_2 concentration solely in San Antonio (peaks in PM_{10} and $PM_{2.5}$ concentrations were observed at San Antonio on 18 Oct., but not on 19 Oct.). Between 21 and 23 Nov., NO_2 24 h-mean concentrations >30 μg/m^3 were observed at El Pilar, accompanied by peaks in the SO_2, $PM_{2.5}$ and PM_{10} 24 h-mean concentrations, while on 23 Nov. NO_2 24 h-mean concentration > 50 μg/m^3 were observed at La Grama, accompanied by a peak in PM_{10} 24 h-mean concentration solely. No significant increase in the NO_2 concentration was observed in San Antonio during this period.

4.3. Particle size distributions of the tephra samples

We observe a clear overall decrease of the median particle size over the course of the eruption at both proximal and distal sites, with some daily and inter-site variation (Fig. 5a, b). Median size ranges from fine (< 63 μm) to very coarse (> 1 mm) ash, with coarse ash dominating at proximal sites (Fig. 5a), and medium ash (500 to 63 μm) for the distal ones (Fig. 5b). Proximal deposits were better sorted (i.e. lower sorting values, Fig. 5c) than distal deposits (Fig. 5d). Sorting shows little spatial or temporal variation at proximal sites (Fig. 5c), but is highly variable in both space and time at distal sites (Fig. 5d). The proportion of fine ash in distal deposits generally ranges from 10 to 90 vol% (Fig. 5f), including up to 8 vol% of particles <10 μm (Fig. 5h). In contrast, fine ash in proximal deposits rarely exceeds 8 wt% (Fig. 5e), with <2 wt% of particles <10 μm (Fig. 5g). No systematic changes of the particle sizes are associated with peaks in sedimentation rates (Fig. 5).

4.4. Satellite observation of the tephra plume dispersion

Tephra plumes from the Tajogaite eruption were visible in MSG-SEVIRI infrared images and MODIS visible images during most of the eruption, except for 5 days when neither dataset was available (Fig. 6 and Table S2 in Supplementary Information). Both datasets generally agree, with plumes detected in the same sectors on the same dates (Fig. 6). Differences arise because MODIS provides only two images per day, which may miss short-lived plumes, and because the MSG-SEVIRI retrieval method cannot detect dilute or water-rich plumes. Due to its

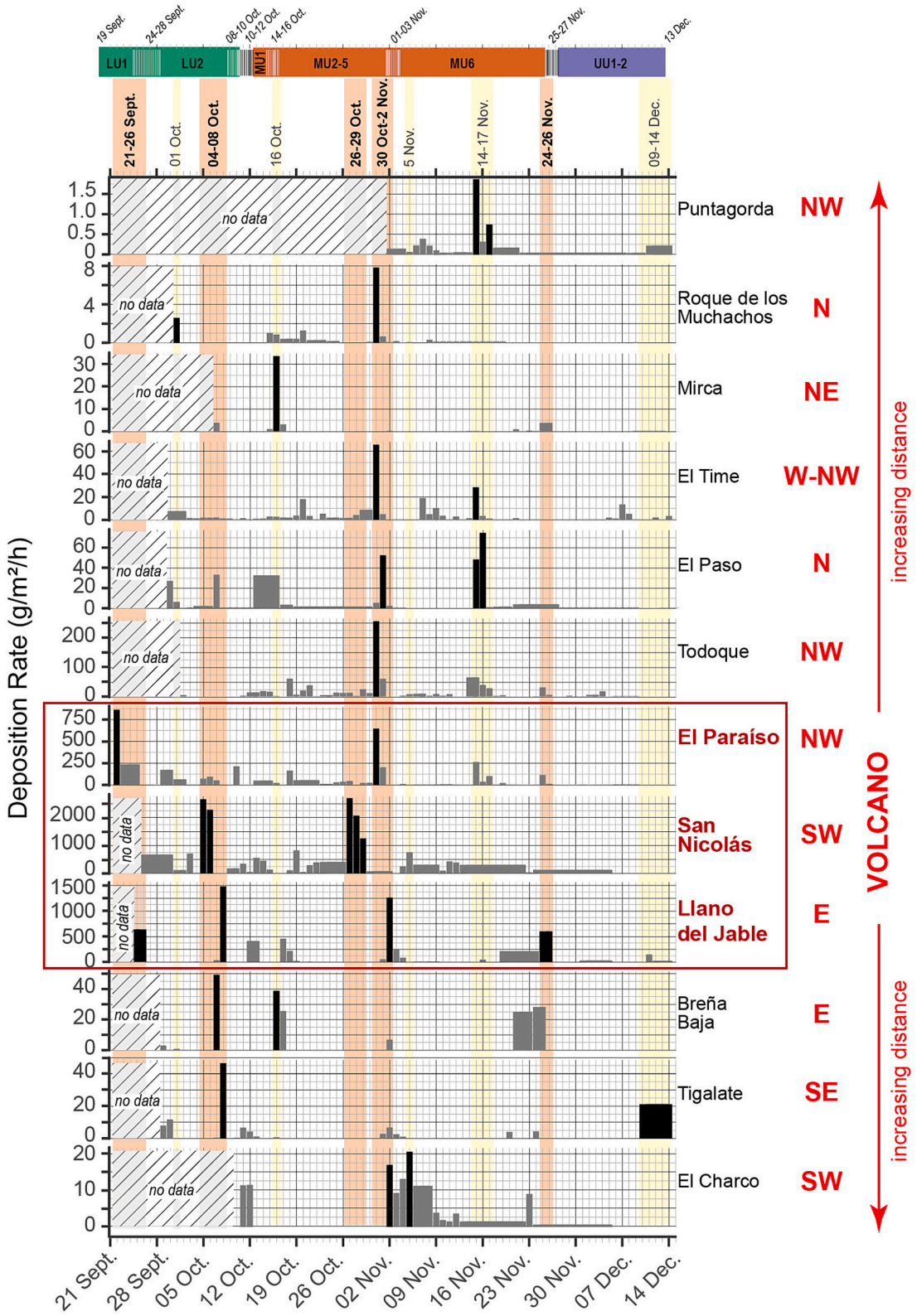

Fig. 2. Tephra deposition rate time-series for the 12 collection sites on La Palma during the 2021 Tajogaite eruption. Minor tick marks on the horizontal axes indicate 00:00 AM. Deposition rate bars straddle tick marks as the collectors were emptied during daylight hours, i.e. straddling midnight. The period preceding the start of data collection are indicated. The three most proximal collection sites (located less than 3 km from vents) are highlighted by the red box. Black bars represent maxima in deposition rates. Orange shaded areas represent periods during which maxima in rates are reached at one or more of the three proximal sites. Yellow shaded areas highlight periods during which maxima in rates are reached at at least one distal site, but which are not accompanied by maxima at the proximal sites. At the top of the figure we show the time-stamped stratigraphic tephra sequence after Bonadonna et al. (2022) indicating the three main units (LU: Lower Unit, MU: Middle Unit, UU: Upper Unit) and subunits identified from field deposits.

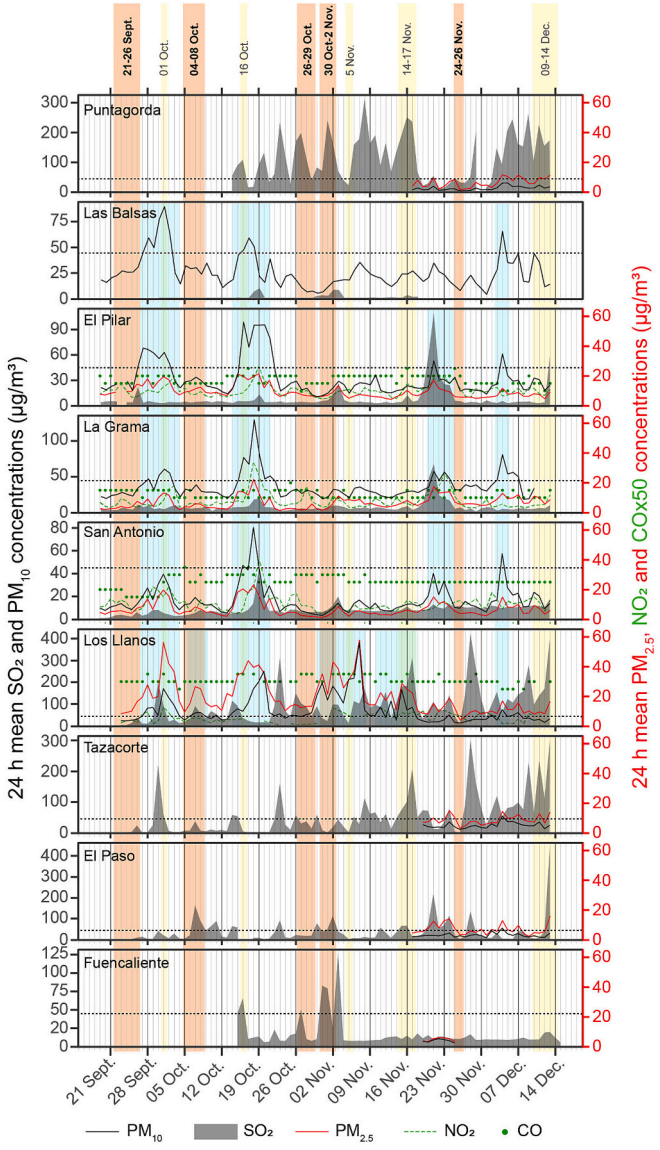

Fig. 3. Variations in air quality recorded at the 9 stations operating during the eruption (see locations in Fig. 1b). Shown are the 24-hour mean ambient air concentrations of SO_2 and PM_{10} (left axis), $PM_{2.5}$, NO_2 and 50 ╳ CO (right axis). Data are from the Government of the Canary Islands regulatory monitoring network (https://www3.gobiernodecanarias.org/medioambiente/calidaddelaire/inicio.do). The dashed black lines mark the World Health Organization air quality guidelines for PM_{10} ambient air concentration (24-hour mean of 45 µg/m^3). As per Fig. 2, orange shaded intervals indicate periods when maxima in deposition rates were observed at one or more proximal sites, and yellow intervals indicate maxima observed at one or more distal sites, without corresponding maxima at proximal sites. Blue shading highlights periods of PM_{10} and $PM_{2.5}$ concentration peaks in the respective station records.

higher spatial resolution, MODIS images allowed the plume shape to be characterized (Table S2), ranging from narrow and elongated to wide or radially symmetric (Table S2). The MSG-SEVIRI time series shows that plume dispersion overLa Palma island was highly dynamic, with its position shifting markedly over short timescales, even within a single day (Fig. 6). The tephra plume was frequently transported over the western half of the island, especially the west and south-west sectors S3 and S5 (Fig. 1), confirmed by both datasets (Fig. 6). However, tephra was also episodically transported over the eastern half of the island (Fig. 6). Finally, satellite-based observations of tephra transport (MSG-SEVERI and MODIS; Fig. 6) match well with tephra deposition (Fig. 2 and Table S6) and PM concentration peaks (Fig. 3 and Table S7).

5. Discussion

5.1. Origin of the spatiotemporal variations of tephra deposition

The variations in tephra deposition rates at the three most proximal collection sites appear to be mainly driven by fluctuations of the tephra eruption rate at the explosive vents (Fig. 2). Given their proximity (< 3 km) and directional distribution around the vents (Fig. 1b), we would expect proximal tephra deposition to be recorded at at least one of these sites regardless of the direction of plume dispersion. Instead, we observe clear periods during which maxima in deposition rates are reached at one of these sites (orange shaded areas in Fig. 2), alternating with periods during which deposition rates are low at all three sites, which can only be driven by variations in the eruption rate at the source. This pattern is well illustrated by the sequence from 27 October and 2 November (Fig. 7c and Table S6). During this interval, wind from the northeast drove high deposition at San Nicolás (SW of the vents) on 26–29 Oct., followed by maxima at El Paraíso (NW of the vents) on 30 Oct.-1 Nov. when the wind came from SSE, and finally at Llano del Jable (E of the vents) on 1–2 Nov. under SSW winds. However, between 29 and 30 October, despite El Paraíso and Llano del Jable being downwind of the plume axis under WSW-SSE winds (Fig. 7c), deposition rates remained low. These observations imply that the eruption rate at the source was low during that period, consistent with inferences from tephra stratigraphy (Bonadonna et al., 2022) and low lava discharge rates (Plank et al., 2023).

From the variations in tephra deposition rates at the proximal sites (Fig. 2 and Table S6), we conclude that the tephra eruption rate (i) fluctuated from day-to-day during the course of the eruption, (ii) attained maxima during the periods 21–26 Sept., 4–8 Oct., 26–29 Oct., 30 Oct.-2 Nov. and 24–26 Nov., and (iii) decreased throughout the course of the eruption, with a marked decline after 2 Nov. These observations are in agreement with stratigraphic studies of the tephra blanket (Bonadonna et al., 2022) and in-situ observations and measurements of eruptive activity (Bonadonna et al., 2023), which demonstrated that the explosive activity was pulsatory, with style variations (ash-poor gas puffing, Strombolian, violent Strombolian, and lava fountaining) on the scale of minutes to hours at single or multiple vents (including co-existing different styles). Interestingly, the periods of high tephra eruption rates identified here (Fig. 2) precede significant shifts of the eruptive style identified in the stratigraphy (Fig. 7a), and concur with increased tremor activity (Bonadonna et al., 2022), as well as changes in tephra properties (Da Mommio et al., 2025). The overall decrease in the intensity of the explosive activity is consistent with the decrease over time of the time-averaged lava discharge rate (Bonadonna et al., 2022; Plank et al., 2023) and of the volcanic gas emission rates (Asensio-Ramos et al., 2025; Burton et al., 2023; Esse et al., 2025; Taquet et al., 2025), suggesting that the magma reservoir depleted during the course of the eruption.

At distal sites, the variations of tephra deposition rates are controlled by the wind speed and direction (Fig. 7c), which influence plume height (Fig. 7b) and its direction (Fig. 2) (Bursik, 2001). Distal maxima in deposition rates are explained by the prevailing wind direction on the day (Table S6). Maxima in deposition rates occurring at distal sites without being associated with increased activity at the vent (as evidenced by low deposition rates at the proximal sites, such as on 1 Oct., 16 Oct., 5 Nov., 14–17 Nov., and 12–14 Dec.; Fig. 2) correspond to periods with low wind (<20 m/s). Weak winds allow tephra plumes to reach high altitudes and hence to disperse tephra to greater distances. This phenomenon is seen on 1 Oct., 16 Oct., and 12–14 Dec. (final climactic phase), when tephra plumes up to 7.5 km above sea level formed (Fig. 7b), and also likely occurred on 5 Nov. and 14–17 Nov., despite lower estimated plume heights (plume height measurements have high uncertainties; Aubry et al., 2021). Our results demonstrate

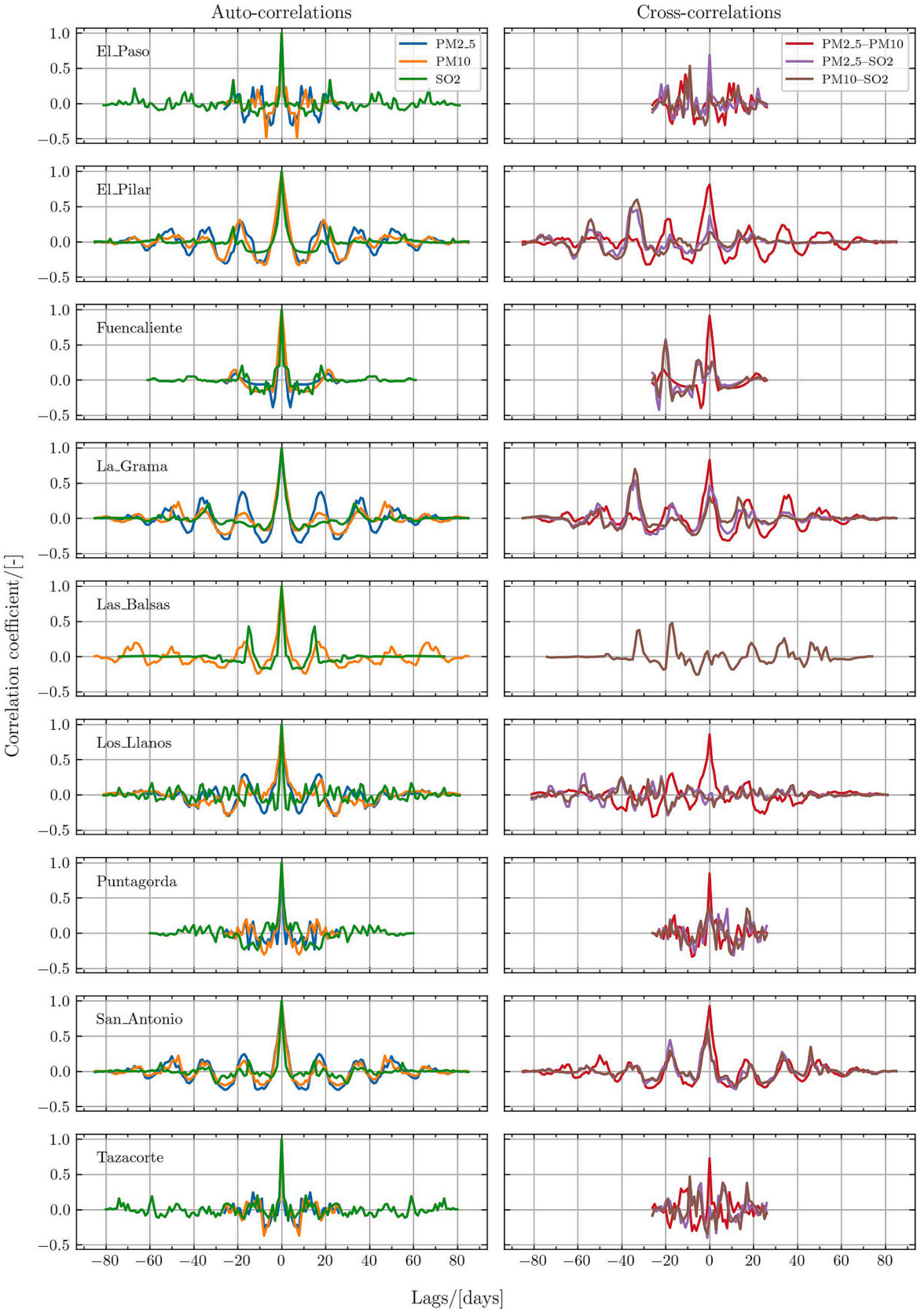

Fig. 4. Auto-correlation and cross-correlation functions of the PM_{10}, $PM_{2.5}$, and SO_2 24-h mean ambient air concentration time-series at the 9 air quality stations in operation during the eruption. Cross-correlation analyses show that the $PM_{2.5}$ and PM_{10} time series are well correlated temporally (correlation coefficient ~1 at 0 days lag) at all the stations. Where complete records of SO_2, PM_{10}, and $PM_{2.5}$ concentrations are available, the correlations between the PM_{10} and SO_2, and $PM_{2.5}$ and SO_2 time-series are poor (correlation coefficient < 0.5 at all lags).

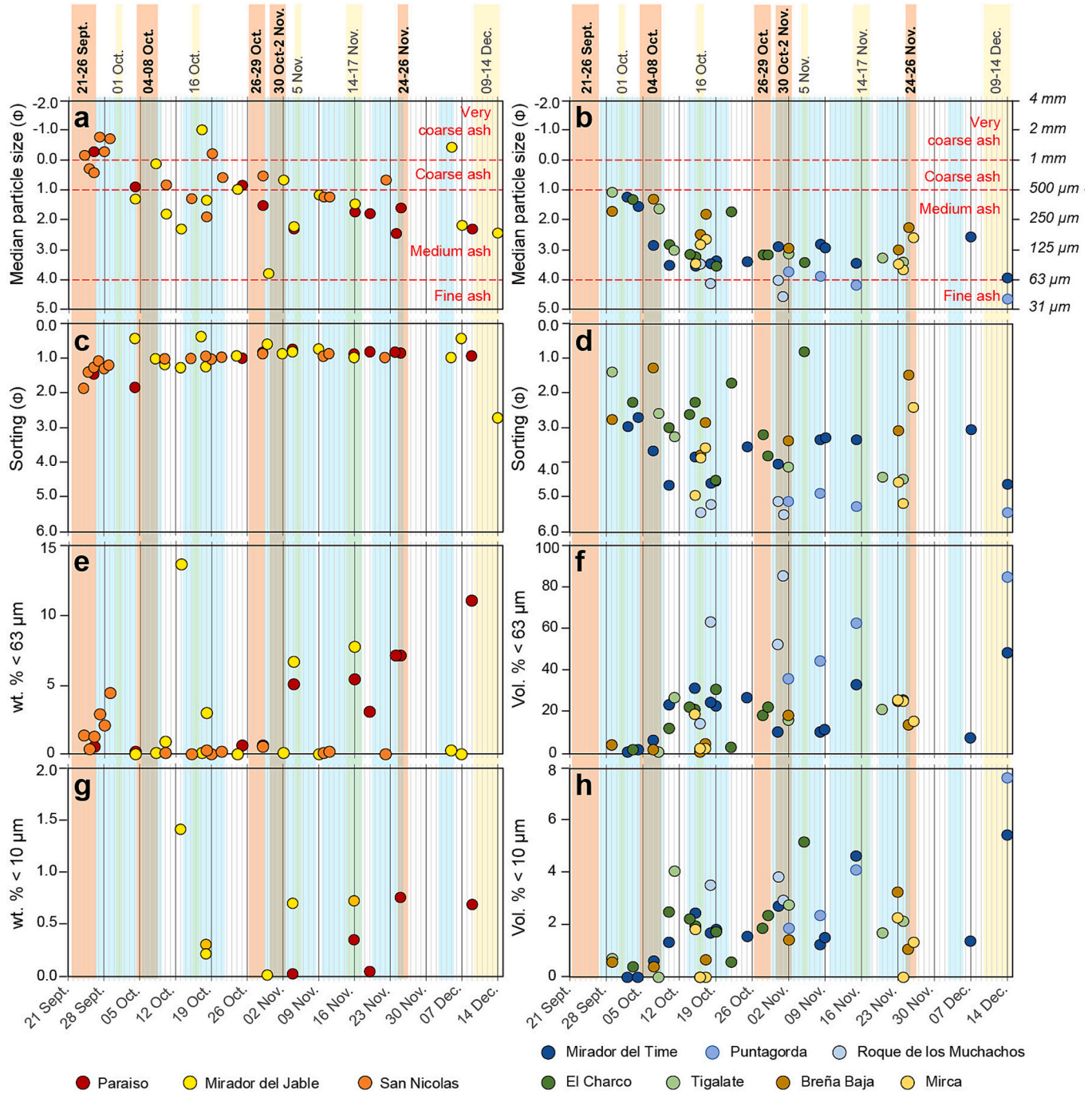

Fig. 5. Evolution of particle size distribution parameters of tephra samples during the eruption at the proximal (< 3 km from vents; left), and distal sites (4–21 km from vents; right): (a-b) median, (c-d) sorting, (e-f) fraction finer than 63 µm (fine ash), (g-h) fraction finer than 10 µm. As per Fig. 2, orange shading marks periods of maximum deposition rates at one or more proximal sites, and yellow shading marks maxima at one or more distal sites, without corresponding proximal maxima. As per Fig. 3, blue shading indicates PM_{10} and $PM_{2.5}$ concentration peaks.

that in medial to distal locations, pulsatory tephra deposition is mainly driven by wind transport, and is less dependent on changes in volcanic activity at the vent. This observation means that during long-lasting, low-intensity eruptions such as at Tajogaite, the intermittent tephra impacts to distal populated areas (not evacuated because beyond the reach of direct deadly impacts) can be best predicted by the meteorological conditions.

5.2. Impact of the tephra emissions on air quality

SO_2 ambient air concentrations during September–December in non-eruptive years (2020, 2022, and 2023; Fig. S2 in Supplementary Information) were very low, confirming that the SO_2 signal during the Tajogaite eruption primarily reflects volcanic gas emissions from vent degassing and of the lava flow field (Asensio-Ramos et al., 2025; Esse et al., 2025; Milford et al., 2023; Taquet et al., 2025).

In contrast, the PM signal during the Tajogaite eruption likely had multiple sources. Peaks in PM_{10} and $PM_{2.5}$ on the Eastern side of La Palma in non-eruptive years (Fig. S2) suggest frequent contributions from Saharan dust outbreaks (i.e. 1 to 2 events per year between September and December; Milford et al., 2023). $PM_{2.5}$ can also form by atmospheric oxidation of SO_2 gas which generates sulfate aerosols at

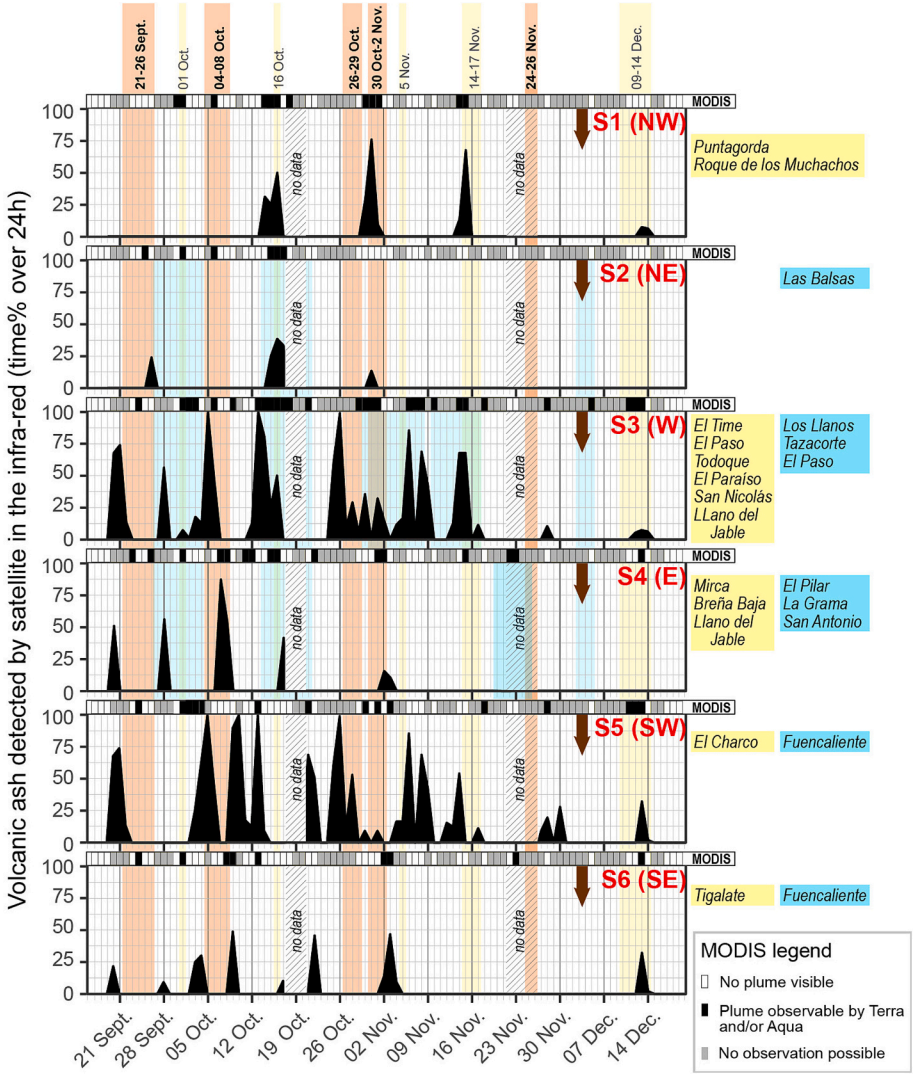

Fig. 6. Variations in tephra plume detections during the eruption, expressed as the percentage of time over 24 h, from MSG-SEVIRI infrared data for each of the sectors of La Palma (S1 to S6, see map in Fig. 1). Periods when meteorological cloud cover prevented detection are indicated as striped "no data" rectangles. The 3–4 Dec. Saharan dust outbreak observed by MSG-SEVIRI is marked with brown vertical arrows. MODIS visible observations from the Terra and Aqua satellites are also shown for each sector. Tephra collection sites (yellow shading and boxes) and air quality stations (blue boxes and shading) located within each sector are shown. Orange shading highlights periods of maximum deposition rates at proximal sites (Fig. 2), yellow shading marks maxima at distal sites without corresponding proximal maxima (Fig. 2), and blue shading indicates PM_{10} and $PM_{2.5}$ concentration peaks (Fig. 3).

rates depending on background atmospheric conditions (i.e. humidity, light; Mather et al., 2003). Air quality data from the four stations where full datasets were available during the eruption (El Pilar, La Grama, San Antonio, and Los Llanos; Table S3) suggests that the PMs measured in the ambient air did not form solely by conversion of SO_2. It is evidenced by the low cross-correlation values at any lag between the SO_2 and $PM_{2.5}$ 24-hour mean ambient air concentration time series (Fig. 4). If SO_2 conversion was primarily responsible for the $PM_{2.5}$ AQ signal, we would expect significant spatiotemporal correlations between the SO_2 and $PM_{2.5}$ time series, either at zero lag or with a time delay due to conversion time in a complex and variable atmosphere (Pattantyus et al., 2018). Instead, $PM_{2.5}$ correlates strongly with PM_{10} (zero lag; Fig. 4), implying a common source. Additionally, the $PM_{2.5}/PM_{10}$ ratios remain below 1 during the eruption (Figs. S3 and S4 in Supplementary Information), indicating the dominance of coarse particles (greater than $PM_{2.5}$ in size) in the PM_{10} signal during the eruption, consistent with geogenic dusts such as volcanic ash or desert dust. Similar ratios (around 0.3–0.4) observed in 2022–2023 at the Eastern AQ stations (Fig. S4) could be due to resuspension of the volcanic ash deposited by the eruption, which remains in the environment for years after (Paredes-Mariño et al., 2022), as well as Saharan dust outbreaks (dominated by coarse PMs; Adebiyi et al., 2023). In contrast, no major PM pollution peaks occurred in 2020 (Fig. S2) yet the $PM_{2.5}/PM_{10}$ ratio was higher than in the years 2021–2023 over the same period (Fig. S4), suggesting a larger anthropogenic contribution. During the eruption, the deviations of the ratio from a baseline (0.2–0.6) occurred on only three instances at Los Llanos, an increase in each case, suggesting an enrichment in $PM_{2.5}$ (yellow vertical bands in Fig. S3) not clearly associated with SO_2 peaks (Fig. 3). The Tajogaite eruption hence differs from basaltic fissure eruptions in Hawaii (e.g., 2018 eruption; Whitty et al., 2020) or Iceland (e.g., 2014–15 Holuhraun eruption; Carlsen et al., 2021), where ambient $PM_{2.5}$ enrichment was largely due to SO_2-to-sulfate aerosol conversion.

In the case of Tajogaite, ambient air PM peaks during the eruption have two main sources, evidenced in the AQ and satellite datasets (Fig. 3). The first is from tephra emissions and the second is from Saharan dust outbreaks. With the exception of the 3–5 December peak, all PM concentration peaks are preceded by or synchronous with maxima in tephra deposition rates (Figs. 2 and 4, Table S7) and plume

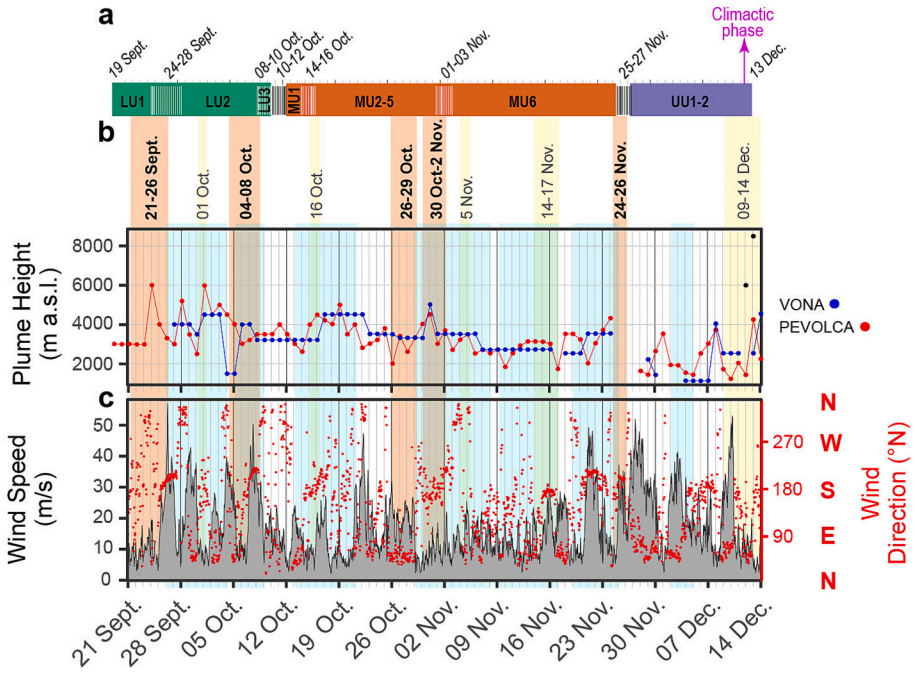

Fig. 7. Qualitative correlation of tephra deposit stratigraphy, plume height above sea level (a.s.l.), wind speed and direction during the eruption. (a) Time-stamped reference stratigraphic section of the eruption, reconstructed post eruption from tephra deposits, showing the three main units (LU: Lower Unit, MU: Middle Unit, UU: Upper Unit) and subunits (Bonadonna et al., 2022). The pink arrow indicates the climactic phase on December 12, which produced plumes >6 km a.s.l. (b) Tephra plume heights from Bonadonna et al. (2022), referring to the PEVOLCA reports (red circles) (https://www.gobiernodecanarias.org/infovolcanlapalma/pevolca/) and the Volcano Observatory Notice for Aviation (VONA; blue circles). Black circles represent the afternoon plumes on 12 and 13 December reported by PEVOLCA. (c) Wind speed (grey shaded area) and wind direction (red circles), measured by AEMET (Agencia Estatal de Meteorologia, Spain) weather station at the Roque de Los Muchachos Astronomical Observatory (1-hour mean data). Orange shading highlights periods of maximum deposition rates at proximal sites (Fig. 2), yellow shading marks maxima at distal sites without corresponding proximal maxima (Fig. 2), and blue shading indicates PM_{10} and $PM_{2.5}$ concentration peaks (Fig. 3).

transport above the corresponding sectors (Fig. 6 and Table S7). This lends further evidence to tephra emissions being a significant, if not the major, source of PMs during these periods. The PM peaks last longer than the periods of high tephra deposition (Fig. 3), which is explained by (i) the persistence in the ambient air of fined-grained volcanic ash (<10 μm) which have low fall velocities and remain coupled to atmospheric circulations (Eychenne and Engwell, 2022), and (ii) the comminution and resuspension by human activity of the tephra deposited on the ground in populated areas (Andronico and Del Carlo, 2016; Tomašek et al., 2026).

There is no unique factor linking the fine particle content of erupted tephra, wind conditions, and PM concentration peaks (Table S7). This demonstrates that wind speed/direction and tephra sizes are secondary drivers of the PM variability due to tephra plumes. Once high amounts of tephra were present in the atmosphere, the PM concentration increased, which impacted given site depending mainly on the direction of transport of the tephra plume (Fig. 6), and its morphology, which varied from very narrow to broad, spread-out shapes (Table S2).

When tephra emissions likely account for PM pollution, a significant peak is systematically measured at the Los Llanos AQ station, except for 20–25 Nov when small PM peaks were recorded at eastern AQ stations only. This anomaly can be explained by high wind speeds (Table S7), producing a narrow plume directed eastwards. At the same time, coincident peaks in PM, SO_2 and NO_2 signals suggest that tephra and gas plumes were well coupled in the atmosphere. The $PM_{2.5}/PM_{10}$ ratio also rose slightly on a few instances during this period (Fig. S2), pointing to a possible contribution of SO_2-to-sulfate aerosol conversion, particularly at the more distant eastern stations. The NO_2 peaks on 20–25 Nov and 14–21 Oct. may also reflect local combustion of biomass or infrastructure (e.g., buildings, roads, plastic cover sheets on banana plantations) burned by the advancing lava flows (Biass et al., 2024; Carracedo et al., 2022). However, the absence of coincident CO peaks argues against combustion being the dominant factor in producing these signals. Whereas the contribution of anthropogenic emissions to PM concentrations during the eruption period cannot be excluded, the temporal correspondence of PM peaks, tephra deposition rate maxima, and tephra plume dispersion directions implies that the eruption is the main driver of variability.

The second source of PM is indicated by the 3–5 Dec. concentration peak, without corresponding tephra emissions (low deposition rates, no plumes observed by satellite; Fig. 3, Fig. 6, Table S7). Satellite imagery shows a Saharan dust outbreak reaching La Palma from the SW at this time (Table S2) which is likely the main source of the PM peak. Saharan dust outbreaks regularly impact the Canary Islands archipelago, with the highest number of episodes between December and January (Milford et al., 2023). In a previous study focusing solely on the AQ data and not accounting for the volcanic activity, Milford et al. (2023) suggested that the 26 Sept.-3 Oct., 7–8 Oct. and 19–21 Oct. 2021 PM peaks at Los Llanos and the Eastern AQ stations were caused by Saharan dust outbreaks based on the observation of a dust layer above Tenerife using Lidar. Our analyses suggest instead that these events were caused by tephra emissions, which have optical properties similar to geogenic dust. This is supported by satellite observations on 7–8 Oct., which show volcanic ash dispersing as far as Tenerife (Table S2).

5.3. *Implications for air quality and human exposure to volcanic PMs during basaltic eruptions*

That the tephra emitted by the Tajogaite eruption generated ambient air PM pollution peaks is a striking and unexpected finding in the context of a basaltic eruption. Low viscosity basaltic magmas are not expected to produce large quantities of fine-grained tephra because of their low fragmentation efficiency (Cashman and Scheu, 2015; Jones et al., 2022). Indeed, the short relaxation time of low viscosity magmas

limit gas bubble overpressure thus reducing the fragmentation efficiency (Cashman and Scheu, 2015). To date, contributions of volcanic ash to PM_{10} and $PM_{2.5}$ pollution detectable by AQ stations have been mostly documented for higher intensity explosive eruptions, such as Córdon Caulle eruption, Chile in 2011 (mass eruption rate of 10^6 to 10^7 kg/s; Bonadonna et al., 2015), which produced PM pollution detected 1600 km away in Uruguay (Balsa et al., 2016), or Eyjafjallajökull eruption, Iceland, in 2010 (mass eruption rate of $\sim 10^4$ kg/s; Dürig et al., 2015), which increased PM concentrations locally and as far as France and Germany (Carlsen et al., 2015; Colette et al., 2011; Schäfer et al., 2011). These eruptions produced sustained ash-laden plumes reaching altitudes greater than 10 km, and fine-grained tephra deposits (Bignami et al., 2014; Bonadonna et al., 2015; Bonadonna et al., 2011). Despite its lower plume height (1 to 6 km a.s.l., Fig. 7) and eruption intensity (tephra mass eruption rate of 3–4 $\times$ 10^3 kg/s; Bonadonna et al., 2022), our results demonstrate that the Tajogaite eruption still produced fine-grained ash in the ranges of PM_{10} and $PM_{2.5}$. Sub-10 μm volcanic ash could have been formed by magmatic fragmentation in the conduit (Jones et al., 2022), abrasion processes due to particle-particle interactions in the lava fountain (Edwards et al., 2020), or by post-depositional comminution (e.g., road traffic), as observed at Etna, Italy (Andronico and Del Carlo, 2016; Tomašek et al., 2026). Tephra particle size (Fig. 5 and Table S7) did not correlate with the PM concentration peaks, suggesting that the tephra deposition rate rather than particle size distribution at the time of deposition is the principal control of the PM concentration amplitude. Secondary comminution processes are probably important to produce the sub-10 μm ash not originally present in the depositing tephra. Yet, the formation of sub-10 μm ash by magmatic fragmentation is an under-documented process, because of such small particle sizes being poorly measured and analysed by traditional volcanological techniques. Hence we cannot overrule that only a small amount of primarily-formed, sub-10 μm ash in the depositing tephra (not easily measured by laser diffraction in a polydispersed sample) is enough to significantly increase PM concentrations. Comparing our findings with other basaltic eruptions with significant tephra emissions (e.g., at Etna and Stromboli in Italy, at Fagradalsfjall in Iceland) is not possible because combining tephra sedimentation records and air quality monitoring data has not been performed before in such settings. Given the valuable insights provided by our analysis of the Tajogaite eruption, implementing similar approaches (i.e. time series tephra collection and satellite observations combined with air quality monitoring) during future basaltic eruptions would be worthwhile to augment the state of knowledge.

Our results provide valuable information for population exposure to volcanic pollution during the Tajogaite eruption. We show that the western central part of the island was much more affected by PM pollution than the eastern and central parts, although major pollution peaks also impacted eastern parts. We demonstrate that SO_2 pollution (and, by implication, other volcanic gas species not documented by AQ data; Asensio-Ramos et al., 2025; Esse et al., 2025; Taquet et al., 2025) followed a similar spatial pattern, implying that populations on the western and northern parts of the island faced the greatest health risks due to combined exposure to PM_{10}, $PM_{2.5}$, and a cocktail of volcanic gases. We also show that the ambient air PM concentration peaks lasted for several days to weeks after an episode of high tephra deposition (Fig. 3). Such prolonged air pollution reflects the resuspension of freshly deposited ash, as observed in Iceland, where windblown "dust storms" cause regular exceedances of WHO PM_{10} guidelines (Carlsen et al., 2015). These are relevant information for any study on the potential impacts on the health of the population (Rodríguez-Pérez et al., 2024).

Attribution of PM pollution peaks to the tephra emissions was done by qualitative correlations of the AQ, tephra deposition and plume dispersion datasets. Discrimination of sources such as volcanic ash and desert dust with similar physical and chemical and hence optical properties, cannot be done based solely on AQ data and atmospheric remote sensing (Milford et al., 2023); volcanological context is essential. In the absence of AQ monitoring, tephra deposition and atmospheric dispersion data provide robust information to approximate the start date and location of PM pollution peaks, but not their amplitude or duration. This underlines the importance of developing robust AQ monitoring networks in active volcanic environments during and after eruptions to manage risks associated with both direct tephra fallout and secondary resuspension.

6. Conclusion

During the 2021 Tajogaite eruption, intense tephra deposition episodes occurred proximally (within 3 km of the vents), primarily driven by increased eruption rates, and distally (4–21 km from the vents) due to wind dispersion. Ambient air PM concentration peaks on La Palma that exceeded WHO guidelines are correlated with these intense tephra deposition episodes and hence attributable to the volcanic emissions. Low-explosivity basaltic eruptions such as the hybrid Tajogaite eruption, characterized by low fragmentation efficiency, can generate ash in the PM_{10} and $PM_{2.5}$ ranges through primary fragmentation processes or comminution and resuspension of deposited tephra. Such fine particles contribute to PM pollution and persist in the ambient air beyond deposition episodes, thereby prolonging population exposure. Tephra emissions were a more significant source of PM than secondary aerosol formation from SO_2, with exposure being consistently higher in the western half of the island. The deconvolution of different PM sources is critical to the quantification of the contribution of tephra emissions and other geogenic and anthropogenic sources to PM loads as volcanic emissions usually occur in multi-source environments, such as was the case at La Palma. Future studies would benefit from chemical analyses of PM such as source-tracer approaches to strengthen source attribution. Finally, our study highlights that volcanological datasets (e.g., tephra deposition rates, tephra characteristics, plume dispersion) are valuable proxies for identifying the onset and spatial extent of volcanic air pollution. However, only AQ monitoring networks can provide robust and reliable information on the amplitude and duration of such air pollution episodes, underscoring their importance for hazard assessment and public health protection in active volcanic regions.

CRediT authorship contribution statement

Julia Eychenne: Writing – review & editing, Writing – original draft, Visualization, Validation, Supervision, Resources, Project administration, Methodology, Investigation, Funding acquisition, Formal analysis, Data curation, Conceptualization. **Raphael Paris:** Writing – review & editing, Writing – original draft, Visualization, Validation, Methodology, Investigation, Formal analysis, Data curation. **Agnès Borbon:** Writing – review & editing, Writing – original draft, Validation, Investigation, Formal analysis, Data curation. **David Jessop:** Writing – review & editing, Writing – original draft, Visualization, Validation, Methodology, Investigation, Formal analysis. **Mathieu Gouhier:** Writing – review & editing, Validation, Methodology, Formal analysis, Data curation. **Guillem Gisbert Pinto:** Writing – review & editing, Validation, Methodology, Formal analysis. **Antoni Calafat:** Writing – review & editing, Resources, Methodology. **Aurélie Colomb:** Writing – review & editing, Validation, Methodology. **José-Luis Fernandez-Turiel:** Writing – review & editing, Validation, Resources, Methodology. **Vincent Gaussen:** Writing – review & editing, Methodology, Formal analysis. **Clara Gorce:** Writing – review & editing, Methodology, Formal analysis. **Séverine Moune:** Writing – review & editing, Validation, Investigation. **Wilman Navarrete:** Writing – review & editing, Methodology, Formal analysis. **Jean-Marie Nedelec:** Writing – review & editing, Resources, Methodology. **Alejandro Rodriguez-Gonzalez:** Writing – review & editing, Resources, Methodology. **Ines Tomašek:** Writing – review & editing, Validation, Methodology, Investigation. **Jon Vilches:** Writing – review & editing, Methodology, Data curation. **Francisco Jose Perez-Torrado:** Writing – review & editing, Resources, Methodology, Data curation.

Declaration of Generative AI and AI-assisted technologies in the writing process

No generative AI has been used for this study and the writing of this manuscript.

Declaration of competing interest

The authors declare that they have no known competing financial interests or personal relationships that could have appeared to influence the work reported in this paper.

Acknowledgments

We are grateful to the PEVOLCA committee for permission to work within the exclusion zone during the 2021 Tajogaite eruption. We are also grateful to Guardas Forestales (Forest Rangers) of Cabildo de La Palma and to a network of volunteers around the island for their invaluable help in collecting tephra materials on a daily basis. We thank Maria Cristo Rodriguez-Perez and Manuel Enrique Fuentes Ferrer for their contribution to the compilation of the air quality dataset and the discussions around these data. This work was funded by the Agence Nationale de la Recherche of the French government through the program "Investissements d'Avenir" (16-IDEX-0001 CAP 20–25). This work is Contribution N°745 of the ClerVolc Program of Excellence of the International Research Centre of Disaster Science and Sustainable Development. Financial support was provided by Grant SD RD 1078/2021 LA PALMA (Monitorización, evaluación y seguimiento multidisciplinar de la erupción volcánica de La Palma - MESVOL) funded by Ministerio de Ciencia e Innovación of Spain to the University of Las Palmas de Gran Canaria, and Grant PGC2018-101027-B-I00, funded by MCIN/AEI/10.13039/501100011033.

Appendix A. Supplementary data

Supplementary data to this article can be found online at https://doi.org/10.1016/j.scitotenv.2026.181551.

Data availability

All the data used in this work are either provided as supplementary information or are available with open access online.

References

Adebiyi, A., Kok, J.F., Murray, B.J., Ryder, C.L., Stuut, J.-B.W., Kahn, R.A., Knippertz, P., Formenti, P., Mahowald, N.M., Pérez García-Pando, C., Klose, M., Ansmann, A., Samset, B.H., Ito, A., Balkanski, Y., Di Biagio, C., Romanias, M.N., Huang, Y., Meng, J., 2023. A review of coarse mineral dust in the Earth system. Aeolian Res. 60, 100849.

Afonso, A., Aparicio, A., Hernández-Pacheco, A., Rodríguez-Badiola, E., 1974. Morphology evolution of Teneguía volcano area. Estudios Geológicos Teneguía 19–26.

Andronico, D., Del Carlo, P., 2016. PM10 measurements in urban settlements after lava fountain episodes at Mt. Etna, Italy: pilot test to assess volcanic ash hazard to human health. Nat. Hazards Earth Syst. Sci. 16 (1), 29–40.

Asensio-Ramos, M., Cofrades, A.P., Burton, M., La Spina, A., Allard, P., Barrancos, J., Hayer, C., Esse, B., D'Auria, L., Hernández, P.A., Padrón, E., Melián, G.V., Pérez, N. M., 2025. Insights into magma dynamics from daily OP-FTIR gas compositions throughout the 2021 Tajogaite eruption, La Palma, Canary Islands. Chem. Geol. 676, 122605.

Aubry, T.J., Engwell, S., Bonadonna, C., Carazzo, G., Scollo, S., Van Eaton, A.R., Taylor, I.A., Jessop, D., Eychenne, J., Gouhier, M., Mastin, L.G., Wallace, K.L., Biass, S., Bursik, M., Grainger, R.G., Jellinek, A.M., Schmidt, A., 2021. The Independent Volcanic Eruption Source Parameter Archive (IVESPA, version 1.0): a new observational database to support explosive eruptive column model validation and development. J. Volcanol. Geotherm. Res. 417, 107295.

Balsa, A.I., Caffera, M., Bloomfield, J., 2016. Exposures to particulate matter from the eruptions of the Puyehue volcano and birth outcomes in Montevideo, Uruguay. Environ. Health Perspect. 124 (11), 1816–1822.

Biass, S., Reyes-Hardy, M.-P., Gregg, C., Di Maio, L.S., Dominguez, L., Frischknecht, C., Bonadonna, C., Perez, N., 2024. The spatiotemporal evolution of compound impacts from lava flow and tephra fallout on buildings: lessons from the 2021 Tajogaite eruption (La Palma, Spain). Bull. Volcanol. 86 (2), 10.

Bignami, C., Corradini, S., Merucci, L., De Michele, M., Raucoules, D., De Astis, G., Stramondo, S., Piedra, J., 2014. Multisensor satellite monitoring of the 2011 Puyehue-Cordon Caulle eruption. IEEE J. Select. Top. Appl. Earth Observ. Remot. Sens. 7 (7), 2786–2796.

Bonadonna, C., Genco, R., Gouhier, M., Pistolesi, M., Cioni, R., Alfano, F., Hoskuldsson, A., Ripepe, M., 2011. Tephra sedimentation during the 2010 Eyjafjallajökull eruption (Iceland) from deposit, radar, and satellite observations. J. Geophys. Res. Solid Earth 116 (B12), B12202.

Bonadonna, C., Cioni, R., Pistolesi, M., Elissondo, M., Baumann, V., 2015. Sedimentation of long-lasting wind-affected volcanic plumes: the example of the 2011 rhyolitic Cordón Caulle eruption, Chile. Bull. Volcanol. 77 (2), 1–19.

Bonadonna, C., Pistolesi, M., Biass, S., Voloschina, M., Romero, J., Coppola, D., Folch, A., D'Auria, L., Martin-Lorenzo, A., Dominguez, L., Pastore, C., Reyes Hardy, M.-P., Rodríguez, F., 2022. Physical characterization of long-lasting hybrid eruptions: the 2021 Tajogaite eruption of Cumbre Vieja (La Palma, Canary Islands). J. Geophys. Res. Solid Earth 127 (11), e2022JB025302.

Bonadonna, C., Pistolesi, M., Dominguez, L., Freret-Lorgeril, V., Rossi, E., Fries, A., Biass, S., Voloschina, M., Lemus, J., Romero, J.E., Zanon, V., Pastore, C., Reyes Hardy, M.-P., Di Maio, L.S., Gabellini, P., Martin-Lorenzo, A., Rodriguez, F., Perez, N. M., 2023. Tephra sedimentation and grainsize associated with pulsatory activity: the 2021 Tajogaite eruption of Cumbre Vieja (La Palma, Canary Islands, Spain). Front. Earth Sci. 11.

Bonelli Rubio, J.M., 1950. Contribución al Estudio de la Erupción del Volcán del Nambroque o San Juan (Isla de La Palma) 24 de Junio – 4 de Agosto de 1949, Talleres del Instituto Geográfico y Catastral. Instituto Geográfico y Catastral, Madrid, pp. 1–22.

Bursik, M., 2001. Effect of wind on the rise height of volcanic plumes. Geophys. Res. Lett. 28 (18), 3621–3624.

Burton, M., Aiuppa, A., Allard, P., Asensio-Ramos, M., Cofrades, A.P., La Spina, A., Nicholson, E.J., Zanon, V., Barrancos, J., Bitetto, M., Hartley, M., Romero, J.E., Waters, E., Stewart, A., Hernández, P.A., Lages, J.P., Padrón, E., Wood, K., Esse, B., Hayer, C., Cyrzan, K., Rose-Koga, E.F., Schiavi, F., D'Auria, L., Pérez, N.M., 2023. Exceptional eruptive CO2 emissions from intra-plate alkaline magmatism in the Canary volcanic archipelago. Commun. Earth Environ. 4 (1), 467.

Carlsen, H.K., Gislason, T., Forsberg, B., Meister, K., Thorsteinsson, T., Jóhannsson, T., Finnbjornsdottir, R., Oudin, A., 2015. Emergency hospital visits in association with volcanic ash, dust storms and other sources of ambient particles: a time-series study in Reykjavík, Iceland. Int. J. Environ. Res. Public Health 12 (4), 4047–4059.

Carlsen, H.K., Ilyinskaya, E., Baxter, P.J., Schmidt, A., Thorsteinsson, T., Pfeffer, M.A., Barsotti, S., Dominici, F., Finnbjornsdottir, R.G., Jóhannsson, T., Aspelund, T., Gislason, T., Valdimarsdóttir, U., Briem, H., Gudnason, T., 2021. Increased respiratory morbidity associated with exposure to a mature volcanic plume from a large Icelandic fissure eruption. Nat. Commun. 12 (1), 2161.

Carracedo, J.C., Troll, V.R., Day, J.M.D., Geiger, H., Aulinas, M., Soler, V., Deegan, F.M., Perez-Torrado, F.J., Gisbert, G., Gazel, E., Rodriguez-Gonzalez, A., Albert, H., 2022. The 2021 eruption of the Cumbre Vieja volcanic ridge on La Palma, Canary Islands. Geol. Today 38 (3), 94–107.

Cashman, K.V., Scheu, B., 2015. Magmatic fragmentation. In: Sigurdsson, H. (Ed.), The Encyclopedia of Volcanoes. Elsevier.

Colette, A., Favez, O., Meleux, F., Chiappini, L., Haeffelin, M., Morille, Y., Malherbe, L., Papin, A., Bessagnet, B., Menut, L., Leoz, E., Rouïl, L., 2011. Assessing in near real time the impact of the April 2010 Eyjafjallajökull ash plume on air quality. Atmos. Environ. 45 (5), 1217–1221.

Da Mommio, S., Voloschina, M., Coldwell, B.C., Pérez, N.M., Bonadonna, C., Pistolesi, M., 2025. Eruptive dynamics of the 2021 Tajogaite eruption (La Palma, Canary Islands) as revealed by the physical and textural characterization of tephra. Bull. Volcanol. 87 (6), 43.

Delmelle, P., Lambert, M., Dufrêne, Y., Gerin, P., Óskarsson, N., 2007. Gas/aerosol–ash interaction in volcanic plumes: new insights from surface analyses of fine ash particles. Earth Planet. Sci. Lett. 259 (1), 159–170.

Delmelle, P., Wadsworth, F.B., Maters, E.C., Ayris, P.M., 2018. High temperature reactions between gases and ash particles in volcanic eruption plumes. Rev. Mineral. Geochem. 84 (1), 285–308.

Dürig, T., Gudmundsson, M.T., Karmann, S., Zimanowski, B., Dellino, P., Rietze, M., Büttner, R., 2015. Mass eruption rates in pulsating eruptions estimated from video analysis of the gas thrust-buoyancy transition—a case study of the 2010 eruption of Eyjafjallajökull, Iceland. Earth Planets Space 67 (1), 180.

Edwards, M.J., Pioli, L., Harris, A.J.L., Gurioli, L., Thivet, S., 2020. Magma fragmentation and particle size distributions in low intensity mafic explosions: the July/August 2015 Piton de la Fournaise eruption. Sci. Rep. 10, 13953. https://doi.org/10.1038/s41598-020-69976-y.

Esse, B., Burton, M., Hayer, C., La Spina, G., Pardo Cofrades, A., Asensio-Ramos, M., Barrancos, J., Pérez, N., 2025. Forecasting the evolution of the 2021 Tajogaite eruption, La Palma, with TROPOMI/PlumeTraj-derived SO2 emission rates. Bull. Volcanol. 87 (3), 20.

Eychenne, J., Engwell, S.L., 2022. The grainsize of volcanic fall deposits: spatial trends and physical controls. GSA Bull. 135 (7-8), 1844–1858. https://doi.org/10.1130/B36275.1.

Freire, S., Florczyk, A.J., Pesaresi, M., Sliuzas, R., 2019. An improved global analysis of population distribution in proximity to active volcanoes, 1975–2015. ISPRS Int. J. Geo Inf. 8 (8), 341.

Guéhenneux, Y., Gouhier, M., 2024. HOTVOLC: the official French satellite-based service for operational monitoring and early warning of volcanic ash plumes. Bull. Volcanol. 86 (4), 29.

Health Effect Institute, 2024. State of Global Air 2024. Special Report. Boston, MA. https://www.stateofglobalair.org/resources/report/state-global-air-report-2024.
Jones, T.J., Cashman, K.V., Liu, E.J., Rust, A.C., Scheu, B., 2022. Magma fragmentation: a perspective on emerging topics and future directions. Bull. Volcanol. 84 (5), 45.
Longpré, M.A., Felpeto, A., 2021. Historical volcanismin the Canary Islands; part 1: a review of precursory and eruptive activity, eruption parameter estimates, and implications for hazard assessment. J. Volcanol. Geotherm. Res. 419, 107363.
Manzella, I., Bonadonna, C., Phillips, J.C., Monnard, H., 2015. The role of gravitational instabilities in deposition of volcanic ash. Geology 43, 211–214.
Martí, J., Castro, A., Rodríguez, C., Costa, F., Carrasquilla, S., Pedreira, R., Bolos, X., 2013. Correlation of magma evolution and geophysical monitoring during the 2011–2012 El Hierro (Canary Islands) submarine eruption. J. Petrol. 54, 1349–1373.
Mather, T., Pyle, D., Oppenheimer, C., 2003. Tropospheric Volcanic Aerosol.
Milford, C., Torres, C., Vilches, J., Gossman, A.-K., Weis, F., Suárez-Molina, D., García, O. E., Prats, N., Barreto, Á., García, R.D., Bustos, J.J., Marrero, C.L., Ramos, R., Chinea, N., Boulesteix, T., Taquet, N., Rodríguez, S., López-Darias, J., Sicard, M., Córdoba-Jabonero, C., Cuevas, E., 2023. Impact of the 2021 La Palma volcanic eruption on air quality: insights from a multidisciplinary approach. Sci. Total Environ. 869, 161652.
Paredes-Mariño, J., Forte, P., Alois, S., Chan, K.L., Cigala, V., Mueller, S.B., Poret, M., Spanu, A., Tomašek, I., Tournigand, P.-Y., Perugini, D., Kueppers, U., 2022. The lifecycle of volcanic ash: advances and ongoing challenges. Bull. Volcanol. 84 (5), 51.
Pattantyus, A.K., Businger, S., Howell, S.G., 2018. Review of sulfur dioxide to sulfate aerosol chemistry at Kīlauea volcano, Hawai'i. Atmos. Environ. 185, 262–271.
Pioli, L., Erlund, E., Johnson, E., Cashman, K., Wallace, P., Rosi, M., Delgado Granados, H., 2008. Explosive dynamics of violent Strombolian eruptions: the eruption of Parícutin Volcano 1943–1952 (Mexico). Earth Planet. Sci. Lett. 271 (1), 359–368.
Plank, S., Shevchenko, A.V., d'Angelo, P., Gstaiger, V., González, P.J., Cesca, S., Martinis, S., Walter, T.R., 2023. Combining thermal, tri-stereo optical and bi-static InSAR satellite imagery for lava volume estimates: the 2021 Cumbre Vieja eruption, La Palma. Sci. Rep. 13, 2057.
Rodríguez-Pérez, M.C., Ferrer, M.E.F., Boada, L.D., Pérez, A.D.A., Aguilar, M.C.D., Jerónimo, J.F.F., Talavera, I.G., Gangotena, L.V., de la Torre, A.H., Simbaña-Rivera, K., de León, A.C., 2024. Health impact of the Tajogaite volcano eruption in La Palma population (ISVOLCAN study): rationale, design, and preliminary results from the first 1002 participants. Environ. Health 23 (1), 19.
Rose, W.I., Durant, A.J., 2011. Fate of volcanic ash: aggregation and fallout. Geology 39 (9), 895–896.
Saxby, J., Beckett, F., Cashman, K., Rust, A., Tennant, E., 2018. The impact of particle shape on fall velocity: implications for volcanic ash dispersion modelling. J. Volcanol. Geotherm. Res. 362, 32–48.
Schäfer, K., Thomas, W., Peters, A., Ries, L., Obleitner, F., Schnelle-Kreis, J., Birmili, W., Diemer, J., Fricke, W., Junkermann, W., Pitz, M., Emeis, S., Forkel, R., Suppan, P., Flentje, H., Gilge, S., Wichmann, H.E., Meinhardt, F., Zimmermann, R., Weinhold, K., Soentgen, J., Münkel, C., Freuer, C., Cyrys, J., 2011. Influences of the 2010 Eyjafjallajökull volcanic plume on air quality in the northern Alpine region. Atmos. Chem. Phys. 11 (16), 8555–8575.
Searl, A., Nicholl, A., Baxter, P.J., 2002. Assessment of the exposure of islanders to ash from the Soufriere Hills volcano, Montserrat, British West Indies. Occup. Environ. Med. 59 (8), 523.
Shatto, C., Weiser, F., Walentowitz, A., Stahlmann, R., Shrestha, S., Guerrero-Campos, M., Medina, F.M., Nogales, M., Jentsch, A., Beierkuhnlein, C., 2024. Volcanic tephra deposition dataset based on interpolated field measurements following the 2021 Tajogaite Eruption on La Palma, Canary Islands, Spain. Data Brief 52, 109949.
Somoza, L., González, F., Barker, S., Madureira, P., Medialdea, T., de Ignacio, C., Lourenço, N., León, R., Vázquez, J., Palomino, D., 2017. Evolution of submarine eruptive activity during the 2011-2012 El Hierro event as documented by hydroacoustic images and remotely operated vehicle observations. Geochem. Geophys. Geosyst. 18, 3109–3137.
Sparks, R.S.J., Bursik, M.I., Ablay, G.J., Thomas, R.M.E., Carey, S.N., 1992. Sedimentation of tephra by volcanic plumes. Part 2: controls on thickness and grain-size variations of tephra fall deposits. Bull. Volcanol. 54 (8), 685–695.
Taddeucci, J., Pompilio, M., Scarlato, P., 2002. Monitoring the explosive activity of the July–August 2001 eruption of Mt. Etna (Italy) by ash characterization. Geophys. Res. Lett. 29 (8).
Taquet, N., Boulesteix, T., García, O., Campion, R., Stremme, W., Rodríguez, S., López-Darias, J., Marrero, C., González-García, D., Klügel, A., Hase, F., García, M.I., Ramos, R., Rivas-Soriano, P., Léon-Luis, S., Carreño, V., Alcántara, A., Sépulveda, E., Milford, C., González-Sicilia, P., Torres, C., 2025. Volatile emissions during the 2021 Cumbre Vieja (La Palma) eruption integrating multiplatform atmospheric observations. Atmos. Chem. Phys. 25 (21), 14591–14628.
Textor, C., Graf, H.-F., Herzog, M., Oberhuber, J.M., 2003. Injection of gases into the stratosphere by explosive volcanic eruptions. J. Geophys. Res. Atmos. 108 (D19).
Tomašek, I., Damby, D.E., Andronico, D., Baxter, P.J., Boonen, I., Claeys, P., Denison, M. S., Horwell, C.J., Kervyn, M., Kueppers, U., Romanias, M.N., Elskens, M., 2021. Assessing the biological reactivity of organic compounds on volcanic ash: implications for human health hazard. Bull. Volcanol. 83 (5), 30.
Tomašek, I., Tournigand, P.Y., Andronico, D., Freret-Lorgeril, V., Eychenne, J., Elizondo, R., Horwell, C., Kueppers, U., Van Mieghem, J., Nuszer, C., taddeucci, J., Claeys, P., Kervyn, M., 2026. Impact of comminution and resuspension of tephra by vehicular activity on ambient PM10 levels in urban areas: insights from a pilot experimental study on Mt. Etna volcano, Italy. Bull. Volcanol. https://doi.org/10.1007/s00445-025-01930-0.
Whitty, R.C.W., Ilyinskaya, E., Mason, E., Wieser, P.E., Liu, E.J., Schmidt, A., Roberts, T., Pfeffer, M.A., Brooks, B., Mather, T.A., Edmonds, M., Elias, T., Schneider, D.J., Oppenheimer, C., Dybwad, A., Nadeau, P.A., Kern, C., 2020. Spatial and temporal variations in SO2 and PM2.5 levels around Kīlauea Volcano, Hawai'i during 2007–2018. Front. Earth Sci. 8.